JHEP

Published for SISSA by Springer

Received: *April 9, 2013*
Accepted: *June 16, 2013*
Published: *July 11, 2013*

Mutual information between thermo-field doubles and disconnected holographic boundaries

Ian A. Morrison[a] **and Matthew M. Roberts**[b]

[a] *DAMTP, Centre of Mathematical Sciences, University of Cambridge, Cambridge, U.K.*

[b] *Department of Physics and Center for Cosmology and Particle Physics, New York University, New York, NY, U.S.A.*

E-mail: i.morrison@damtp.cam.ac.uk, matthew.roberts@nyu.edu

Abstract: We use mutual information as a measure of the entanglement between 'physical' and thermo-field double degrees of freedom in field theories at finite temperature. We compute this "thermo-mutual information" in simple toy models: a quantum mechanics two-site spin chain, a two dimensional massless fermion, and a two dimensional holographic system. In holographic systems, the thermo-mutual information is related to minimal surfaces connecting the two disconnected boundaries of an eternal black hole. We derive a number of salient features of this thermo-mutual information, including that it is UV finite, positive definite and bounded from above by the standard mutual information for the thermal ensemble. We relate the construction of the reduced density matrices used to define the thermo-mutual information to the Schwinger-Keldysh formalism, ensuring that all our objects are well defined in Euclidean and Lorentzian signature.

Keywords: Holography and condensed matter physics (AdS/CMT), Gauge-gravity correspondence, Black Holes

ArXiv ePrint: 1211.2887

doi:10.1007/JHEP07(2013)081

JHEP07(2013)081

Contents

JHEP07(2013)081

1 Introduction

Mutual information (MI) provides a valuable measure of the entanglement of a quantum system. Unlike the von Neumann entanglement entropy of spatial regions, mutual information does not generically suffer UV divergences in quantum field theory (QFT). The mutual information between two subregions A and B describes the total correlation, both classical and quantum, between the regions [1]; in particular, the mutual information provides an upper bound on the correlation for any two observables supported in A and B respectively [2]. As a result the mutual information may be used to ascertain basic properties of any local observable in a quantum system.

Unfortunately, a practical method of computing MI for arbitrary regions in a generic QFT does not exist, making detailed analysis of MI in systems of interest quite difficult. Exact analytic computations of MI are rare and often rely heavily on conformal symmetry (see e.g. [3–5] and references therein). Following the conjecture of Ryu and Takayanagi [6] it is widely believed that the AdS/CFT correspondence can be used to compute quantum informatics quantities in certain strongly coupled QFTs. In particular, it is believed that

the Ryu-Takayanagi (RT) formula [6] for the holographic entanglement entropy captures the leading N^2 contribution the entanglement entropy of the dual CFT. Efforts have been made towards a concrete derivation of the RT formula (see, e.g., [6–10]) but this formula and its covariant formulation [11] remain a conjecture. Furthermore, currently there does not exist a tractable method for calculating subleading corrections to the RT formula (see for instance [9]). However, the robustness of the RT formula has inspired a great deal of investigation into the relationship between quantum information and holography [12–15].

In this paper we examine the holographic mutual information between regions on disconnected boundaries in the maximally extended eternal Schwarzschild-AdS spacetime. The standard holographic interpretation of asymptotically AdS spacetimes with multiple disconnected boundaries is that they provide a bulk realization of an entangled state in a system of multiple non-interacting field theories.[1] In the simplest case of a maximally extended Schwarzschild-AdS black hole, which has two causally disconnected boundaries, one can interpret one boundary as the thermo-field double of the field theory on the second boundary [17]. Therefore, the mutual information we study holographically should characterize the mutual information between operators and their thermo-field double — we call this type of mutual information "thermo-mutual information" so as to distinguish it from mutual information for purely 'physical' operators. The thermo-mutual information quantity provides information about the level of entanglement of the thermal system. It is our hope that this work will lay necessary foundation for a more broad study of holographic mutual information between regions on disconnected boundaries of bulk spacetimes.

As a warm-up to our analysis of holographic systems, we compute the mutual information between 'physical' fields and their thermo-field doubles in two simple systems: a quantum mechanical two-site spin chain and a two-dimensional massless fermion. We then calculate thermo-mutual information for a 2d holographic system dual to asymptotically AdS_3 spacetime in the simple case of a non-rotating BTZ black hole. We find similar behavior in these three very different systems.

The rest of the paper is organized as follows. Section 2 is devoted to introducing thermo-mutual information in the setting of quantum field theory without regard to holographic duals. We begin by briefly reviewing mutual information and thermal quantum systems in section 2.1 and section 2.2 respectively; we then define thermo-mutual information and describe its basic attributes in section 2.3. We provide two example calculations of TMI: the first in the comfortable setting of a quantum mechanical spin chain (section 2.4), and the second, after describing some computational details in section 2.5 (some derivations are in appendix A for brevity), in a 2D CFT (section 2.6). Section 3 is devoted to studying holographic systems. We first review the conjecture of Ryu and Takayanagi in, and give a brief summary of the non rotating BTZ geometry, laying out the tools which make our calculation straightforward. The explicit calculation of mutual information and thermo-mutual information is in section 3.2. We close with a discussion and comments on generalizations of our calculations in section 4.

[1] The robustness of this interpretation is debated [16].

JHEP07(2013)081

2 Thermo-mutual information in field theory

Unless stated otherwise, throughout this section we consider QFTs on a space $\mathcal{M} = \mathbb{R} \times \Lambda$ with $\mathbb{R}$ the continuous time and Λ a $(d-1)$-dimensional spatial lattice with spacing a, which we may simply take to be square. The QFT has a Hilbert space $\mathcal{H}$ and an algebra of local observables $\mathcal{A}(\mathcal{M})$ represented by bounded operators on $\mathcal{H}$. The reason for considering a lattice theory is that for such theories the Hilbert space that is explicitly a direct product of the Hilbert space at each site, $\mathcal{H} = \otimes_\Lambda \mathcal{H}_{site}$, and therefore may be decomposed into spatial regions. The support of a local observable may be as small as a single lattice site labelled by the position vector x. We expect to be able to address continuum QFTs by taking the $a \to 0$ limit; more carefully, we could say that we define a continuum QFT by this limit.

2.1 Mutual information

Mutual information is constructed from reduced density matrices, so we begin by discussing these objects. Quite in general a quantum state Ψ may be described by its density matrix $\rho := \rho(\Psi; \mathcal{A}(\mathcal{M}))$. The lengthy notation denotes that ρ is properly defined as a functional on $\mathcal{A}(\mathcal{M})$ which defines the state Ψ. Correlation functions of an observable $\mathcal{O} \in \mathcal{A}(\mathcal{M})$ with respect to Ψ may be computed by tracing against ρ:

$$\langle \mathcal{O} \rangle_\Psi := \mathrm{tr}_\mathcal{H}[\rho\, \mathcal{O}]. \tag{2.1}$$

However, if we restrict our attention to observables supported in a subset $A \subset \Sigma_t$ with Σ_t an equal-time slice on $\mathcal{M}$, then we may compute correlation functions without knowing ρ in its entirety; it suffices to have the reduced density matrix $\rho_A := \rho(\Psi; \mathcal{A}(A))$. Due to the underlying lattice structure of $\mathcal{M}$ the Hilbert space may be factorized in position space, i.e. $\mathcal{H} = \mathcal{H}_A \times \mathcal{H}_{\overline{A}}$ where $\overline{A}$ is the complement of A on Σ_t. Then ρ_A is obtained by tracing over $\mathcal{H}_{\overline{A}}$:

$$\rho_A = \mathrm{tr}_{\mathcal{H}_{\overline{A}}}[\rho]. \tag{2.2}$$

Correlation functions of any observable $\mathcal{O}_A \in \mathcal{A}(A)$ may then be obtained from operations in $\mathcal{H}_A$ alone via

$$\langle \mathcal{O}_A \rangle_\Psi = \mathrm{tr}_{\mathcal{H}_A}[\rho_A \mathcal{O}_A]. \tag{2.3}$$

The mutual information for two disjoint subsets $A, B \subset \Sigma_t$ is given by

$$\mathrm{MI}(A:B) := S(\rho_A) + S(\rho_B) - S(\rho_{A\cup B}) \geq 0, \tag{2.4}$$

where $S(\rho)$ is the entanglement entropy (a.k.a. Von Neumann entropy) associated to a density matrix:

$$S(\rho) := -\mathrm{tr}[\rho \log \rho]. \tag{2.5}$$

The trace is over the Hilbert space for which ρ is a trace operator. The final inequality in (2.4) is a consequence of the fact that entanglement entropy satisfies strong subadditivity, i.e.,

$$S(A) + S(B) \geq S(A \cup B). \tag{2.6}$$

JHEP07(2013)081

Mutual information quantifies the total correlation, both classical and quantum, between the subsets A and B [1]. This is seen, for instance, in the Pinsker inequality [2]:

$$\mathrm{MI}(A:B) \geq \frac{1}{2}\left(\frac{\langle \mathcal{O}_A \mathcal{O}_B\rangle_\Psi - \langle \mathcal{O}_A\rangle_\Psi \langle \mathcal{O}_B\rangle_\Psi}{||\mathcal{O}_A||||\mathcal{O}_B||}\right)^2, \quad \mathcal{O}_A \in \mathcal{A}(A),\ \mathcal{O}_B \in \mathcal{A}(B). \tag{2.7}$$

Mutual information may be defined for continuum QFTs by taking the limit $a \to 0$. In this limit the entanglement entropy $S(\rho)$ is UV divergent, under reasonable conditions [18] scaling as $S(\rho_A) \sim \mathrm{Area}(\partial A)/a^{d-2} + \ldots$. For $d = 2$ QFTS, which will be what we study in detail, the divergent part of $S(\rho)$ has the universal scaling behavior

$$S(\rho_A) \sim \gamma c N \log a. \tag{2.8}$$

Here γ is a constant which depends on the theory but not the specifics of the region A, c is number which characterized the "number of effective degrees of freedom" (i.e. the central charge in a CFT), and N is the number of boundary points of A. As a result of this universal behavior we may construct a UV-finite symmetric function [19]:

$$F(A:B) = S(\rho_A) + S(\rho_A) - S(\rho_{A\cup B}) - S(\rho_{A\cap B}). \tag{2.9}$$

The mutual information agrees with this function within MI's domain of definition $A \cap B = \emptyset$. Similar statements a believed to hold generically in higher dimensions as well, as all divergent terms are expected to be expressible as integrals over ∂A that only depend on the cutoff scale and therefore should cancel — see discussion in [4, 20, 21] — though these statements are tempered by the fact that there exist few exact calculations of entanglement entropy.

2.2 Thermal systems

The canonical description of thermal states in QFT follows from the semi-classical interpretation of these states as equilibrium states in a grand canonical ensemble. Consider a system governed by a time-independent Hamiltonian H. The thermal state Ω with inverse temperature β is defined by a density matrix $\rho = e^{-\beta H}$; normalized correlations functions of the state are constructed via:

$$\langle \phi(x)\ldots\rangle_\Omega := \frac{1}{Z}\mathrm{tr}[\rho\phi(x)\ldots] = \frac{1}{Z}\mathrm{tr}[e^{-\beta H}\phi(x)\ldots], \tag{2.10}$$

where $Z := \mathrm{tr}[\rho]$ so that $\langle 1\rangle_\Omega = 1$. This description of Ω provides a simple connection to classical statistical mechanics.

However, it is often preferable to describe Ω as a pure rather than mixed state. This may be accomplished with the formalism now known as "thermo-field dynamics" (TFD) — original works include [22, 23], for useful reviews see [24, 25]. TFD employs an enlarged quantum system composed of two copies of the original Hilbert space $\mathcal{H}$. The total Hilbert space of this system is given by the tensor product

$$\mathcal{H}_{\mathrm{TFD}} = \mathcal{H}_1 \otimes \mathcal{H}_2, \tag{2.11}$$

with $\mathcal{H}_1$, $\mathcal{H}_2$ isomorphic to $\mathcal{H}$. The total Hamiltonian is

$$H_{\mathrm{TFD}} = H_1 \otimes 1_2 - 1_1 \otimes H_2, \tag{2.12}$$

JHEP07(2013)081

and Ω may be written in the product space as

$$|\Omega\rangle = \frac{1}{\sqrt{Z}} \sum_n e^{-\beta E_n/2} |E_n\rangle_1 \otimes |E_n\rangle_2, \tag{2.13}$$

where $|E_n\rangle_i$ are eigenstates of H_i belonging to $\mathcal{H}_i$ respectively. From (2.12) and (2.13) we readily see that $H_{\rm TFD}|\Omega\rangle = 0$. For every operator $\phi(x)$ of the original theory there are two copies $\phi_1(x)$, $\phi_2(x)$ in the 'purified' theory. Correlators involving only type-1 operators reproduce correlators of the original theory, e.g.,

$$\langle\Omega|\phi_1(x)\phi_1(y)\ldots|\Omega\rangle = \langle\phi(x)\phi(y)\ldots\rangle_\Omega. \tag{2.14}$$

Since the Hamiltonian does not mix operators on $\mathcal{H}_1$ and $\mathcal{H}_2$, all type-1 operators commute with all type-2 operators:

$$\langle\Omega|\ldots[\phi_1(x),\phi_2(y)]\ldots|\Omega\rangle = 0. \tag{2.15}$$

The algebra of observables of the TFD system is

$$\mathcal{A}_{\rm TFD}(\mathcal{M}) := \mathcal{A}_1(\mathcal{M}) \otimes \mathcal{A}_2(\mathcal{M}). \tag{2.16}$$

It is not always conventional to regard type-2 operators as "observable." Because correlators of type-1 operators reproduce correlators of the original theory, the second copy of the field theory is sometimes referred to as just a 'useful fiction' or computational trick. Furthermore, correlators of exclusively type-2 operators may be related to correlators of exclusively type-1 operators via an anti-unitary map. Ultimately, our motivation for placing the type-2 operators on equal footing with those of type-1 originates from the dual description in terms of eternal black hole spacetimes where the two types of fields live democratically.

2.3 Thermo-mutual information

We can now define the thermo-mutual information (TMI). Consider two subsets $A, B \subset \Sigma_t$ and the associated sub-algebras of observables $\mathcal{A}_1(A) \in \mathcal{A}_1(\mathcal{M})$ and $\mathcal{A}_2(B) \in \mathcal{A}_2(\mathcal{M})$. Using these ingredients we may construct the reduced density matrices

$$\rho_{A1} := \rho(\Omega; \mathcal{A}_1(A)) \tag{2.17}$$

$$\rho_{B2} := \rho(\Omega; \mathcal{A}_2(B)) \tag{2.18}$$

$$\rho_{A1\cup B2} := \rho(\Omega; \mathcal{A}_1(A) \cup \mathcal{A}_2(B)). \tag{2.19}$$

Since $\mathcal{H}_i$ may be factorized in position space we may decompose $\mathcal{H}_1 = \mathcal{H}_{A1} \otimes \mathcal{H}_{\overline{A1}}$, etc; then these density matrices are simply

$$\rho_{A1} = {\rm tr}_{\mathcal{H}_{\overline{A1}}} {\rm tr}_{\mathcal{H}_2} \rho, \tag{2.20}$$

$$\rho_{B2} = {\rm tr}_{\mathcal{H}_1} {\rm tr}_{\mathcal{H}_{\overline{B2}}} \rho, \tag{2.21}$$

$$\rho_{A1\cup B2} = {\rm tr}_{\mathcal{H}_{\overline{A1}}} {\rm tr}_{\mathcal{H}_{\overline{B2}}} \rho. \tag{2.22}$$

JHEP07(2013)081

The first two density matrices correspond to reduced density matrices of the type considered in section 2.1; the third is a hybrid. We define the thermo-mutual information to be:

$$\mathrm{TMI}(A_1 : B_2) := S(\rho_{A1}) + S(\rho_{B2}) - S(\rho_{A1\cup B2}). \tag{2.23}$$

TMI has the same structure as MI but we reserve the notation MI to refer to the case where the two subalgebras $\mathcal{A}_i(A)$, $\mathcal{A}_j(B)$ belong to the same sector $i = j$. We could equivalently define TMI with the structure of the function $F(A : B)$ (2.9) as the last term $S(\rho_{A1\cap B2})$ vanishes due to the fact that $\mathcal{A}_1(A) \cap \mathcal{A}_2(B) = 0$.

Thermo-Mutual information is indeed a kind of mutual information. In particular:

i) **TMI is non-negative:** since $\mathcal{A}_1(A)$ and $\mathcal{A}_2(B)$ are independent their associated density matrices satisfy strong subadditivity (2.6) and thus

$$\mathrm{TMI}(A_1 : B_2) \geq 0. \tag{2.24}$$

ii) **TMI bounds local correlators between A and B:** this is once again a result of the Pinsker inequality. For $\mathcal{O}_{A1} \in \mathcal{A}_1(A)$ and $\mathcal{O}_{B2} \in \mathcal{A}_2(B)$ the Pinsker inequality yields the bound

$$I(A_1 : B_2) \geq \frac{1}{2}\left(\frac{\langle \mathcal{O}_{A1}\mathcal{O}_{B2}\rangle_\Omega - \langle \mathcal{O}_{A1}\rangle_\Omega \langle \mathcal{O}_{B2}\rangle_\Omega}{||\mathcal{O}_{A1}||||\mathcal{O}_{B2}||}\right)^2. \tag{2.25}$$

Other salient features of TMI are:

iii) **TMI provides a lower bound for MI:** when A and B are disjoint the following inequality holds:

$$\mathrm{MI}(A_1 : B_1) - \mathrm{TMI}(A_1 : B_2) = S(A_1 \cup B_2) - S(A_1 \cup B_1) \geq 0. \tag{2.26}$$

This is a simple consequence of the fact that the tensor product $\mathcal{A}_1(A) \otimes \mathcal{A}_2(B)$ is always equally or more disordered than $\mathcal{A}_1(A) \otimes \mathcal{A}_1(B)$. While we do not have an explicit proof of this, it holds in all cases we study, and likely follows simply from subadditivity and the explicit form of the thermo-field double state.

iv) **TMI is free of UV singularities:** just as with mutual information and the F function, in the limit $a \to 0$ the entanglement entropies in (2.23) have UV divergences. So long as the UV divergences are indeed universal and geometric as described in section 2.1, these divergences cancel within $\mathrm{TMI}(A_1 : B_2)$ for all subsets A and B, even when $A \cap B \neq 0$. To see this note the following two facts. First, the "number of effective degrees of freedom" in the type-1 and type-2 sectors are equal. Second, because $\mathcal{A}(A_1)$ and $\mathcal{A}(B_2)$ are independent the geometric region relevant to the divergent terms in $S(\rho_{A1\cup B2})$ is $\mathrm{vol}(\partial A + \partial B)$ rather than $\mathrm{vol}(\partial(A \cup B))$ as in the case of MI.

v) **TMI is bounded above for $\beta > 0$:** this follows from (3) and (4) provided that the theory does not suffer divergences associated to large separations (infrared divergences). The $\beta \to 0$ limit is discussed below.

JHEP07(2013)081

vi) **TMI is non-zero for some A, B:** this is a trivial corollary of (2), and is necessary for Ω to be entangled. Assuming $0 < \beta < \infty$ then Ω does not factorize into a product state on $\mathcal{H}_{\rm TFD}$ Assuming $\mathcal{A}(\mathcal{M})$ is non-empty, then there exists an observable $\mathcal{O}$ such that $\langle \mathcal{O}_1 \mathcal{O}_2 \rangle_\Omega > 0$.

We also note the asymptotic behavior of TMI as $\beta \to \infty$ and $\beta \to 0$:

vii) **TMI vanishes as $\beta \to \infty$ (temperature $T \to 0$):** in this limit the canonical ensemble becomes a pure state of lowest energy; equivalently, in the TFD formalism $\Omega \to |E_0\rangle_1 \otimes |E_0\rangle_2$. Pure states have maximal correlation, so in this limit the mutual information tends to its maximum value. In contrast, the TMI tends to zero in this limit because the type-1 and type-2 sectors are no longer entangled.

viii) **The $\beta \to 0$ ($T \to \infty$) limit:** in this limit the canonical ensemble becomes random and there are no (connected, normalized) correlations. For disjoint regions both the MI and TMI tend to zero (with the MI bounding the TMI from above). When the regions overlap we generically find that the TMI diverges as $\beta \to 0$. This does not contradict the points above.

We may summarize these points by stating that TMI provides a robust measure of the correlation between type-1 and type-2 fields. Two important roles of the TMI($A_1 : B_2$) are that it bounds from below the MI($A : B$), and it bounds from above the correlation between any pair of observables in $\mathcal{A}_1(A)$ and $\mathcal{A}_2(B)$.

2.4 Example in quantum mechanics: the two-spin system

As a first introduction to TMI let us consider an example in the simple setting of quantum mechanics. Consider a system of two "sites" each with a two-spin degree of freedom governed by the Hamiltonian

$$H = \vec{S}_A \cdot \vec{S}_B. \tag{2.27}$$

The sites are labelled A and B and the spin vector $\vec{S}_A = (S_A^x, S_A^y, S_A^z)$ and likewise for $\vec{S}_B$. More details than one could ever want to know about this system can be found in any good quantum mechanics textbook (e.g., ch. 3 of [26]). Each site has two states which we label by the eigenvalues $\pm$ of S_A^z, S_B^z, and so the two-site system has four tensor-product states. The energy eigenkets of the system are[2]

$$\begin{aligned}
|\alpha_1\rangle &= \tfrac{1}{\sqrt{2}}\Big(|+\rangle_A \otimes |-\rangle_B - |-\rangle_A \otimes |+\rangle_B\Big), && E_1 = -3,\\
|\alpha_2\rangle &= \tfrac{1}{\sqrt{2}}\Big(|+\rangle_A \otimes |-\rangle_B + |-\rangle_A \otimes |+\rangle_B\Big), && E_2 = 1,\\
|\alpha_3\rangle &= |+\rangle_A \otimes |+\rangle_B, && E_3 = 1,\\
|\alpha_4\rangle &= |-\rangle_A \otimes |-\rangle_B, && E_4 = 1.
\end{aligned} \tag{2.28}$$

We first consider the system as a canonical ensemble. The density matrix describing the thermal state Ω with inverse temperature β is

$$\rho = \frac{e^{-\beta H}}{Z} = \sum_{n=1}^{4} \frac{e^{-\beta E_n}}{Z} |\alpha_n\rangle\langle\alpha_n|, \quad Z = \sum_{n=1}^{4} e^{-\beta E_n} = e^{3\beta} + 3e^{-\beta}. \tag{2.29}$$

[2]The energy eigenkets correspond to the simultaneous eigenkets of $(\vec{S}_A + \vec{S}_B)^2$ and $(S_A^z + S_B^z)$.

JHEP07(2013)081

The entanglement entropy of the entire system is just the thermodynamic entropy which is easily computed:

$$S(\rho) = \frac{1}{3+e^{4\beta}}\left\{3\log(3+e^{4\beta}) - e^{4\beta}\log\left(1-\frac{3}{3+e^{4\beta}}\right)\right\}. \tag{2.30}$$

If we trace of one of the sites then we are left with a random ensemble; the reduced density matrix is (in the spin basis) is $\rho_A = \mathrm{diag}\{1/2, 1/2\}$. The entanglement entropy of a single site is therefore

$$S(\rho_A) = S(\rho_B) = \log 2. \tag{2.31}$$

From (2.30) and (2.31) we obtain the mutual information $\mathrm{MI}(A:B) = 2\log 2 - S(\rho)$.

Now let us apply the TFD formalism to the system. The state Ω becomes an entangled pure state

$$|\Omega\rangle = \frac{1}{\sqrt{Z}}\sum_{n=1}^{4} e^{-\beta E_n}|\alpha_n\rangle_1 \otimes |\alpha_n\rangle_2, \tag{2.32}$$

To compute the TMI we need the density matrix for $A_1 \cup B_2$; it is a straightforward if aggravating exercise to trace over the B_1 and A_2 spin sites in order to obtain this density matrix. This matrix is not diagonal in the $A_1 \otimes B_2$ spin basis, but is easily diagonalized. The entanglement entropy may then be computed:

$$\begin{aligned} S(\rho_{A1\cup B2}) = -\frac{1}{4(3+e^{4\beta})}\Bigg\{&(-3+e^{2\beta})^2\log\left[\frac{(-3+e^{2\beta})^2}{4(3+e^{4\beta})}\right] \\ &+ 3(1+e^{2\beta})^2\log\left[\frac{\cosh^2(\beta)}{4\cosh(2\beta)-2\sinh(2\beta)}\right]\Bigg\}, \end{aligned} \tag{2.33}$$

and from this we obtain $\mathrm{TMI}(A_1:B_2) = 2\log 2 - S(\rho_{A1\cup B2})$.

We plot $\mathrm{MI}(A_1:B_1)$ and $\mathrm{TMI}(A_1:B_2)$ as a function of β in figure 1. All features of this plot are as anticipated:

i) The TMI bounds the MI from below; this may be analytically verified by examining the quantity

$$\mathrm{MI}(A_1:B_1) - \mathrm{TMI}(A_1:B_2) = -S(\rho) + S(\rho_{A1\cup B2}) \geq 0, \tag{2.34}$$

with $S(\rho)$ and $S(\rho_{A1\cup B2})$ as in (2.31) and (2.33).

ii) Also plotted in figure 1 are the right-hand sides of the Pinsker inequalities (2.7) and (2.25) for the observables $S^z_{A1}S^z_{B1}$ and $S^z_{A1}S^z_{B2}$. For the case at hand these are simply

$$\frac{1}{2}\left(\langle S^z_{A1}S^z_{B1}\rangle_\Omega\right)^2 = \frac{(e^{4\beta}-1)^2}{2(e^{4\beta}+3)^2}, \quad \frac{1}{2}\left(\langle S^z_{A1}S^z_{B2}\rangle_\Omega\right)^2 = \frac{2(e^{2\beta}-1)^2}{(e^{4\beta}+3)^2}. \tag{2.35}$$

These are examples of observables bounded above by the MI and TMI respectively.

iii) In the $\beta \to 0$ limit both the MI and TMI tend to 0 (recall point (8) of section 2.3).

iv) In the $\beta \to \infty$ limit the mutual information tends to its maximal value of $2\log 2$ while the TMI tends to zero (recall point (7) of section 2.3).

JHEP07(2013)081

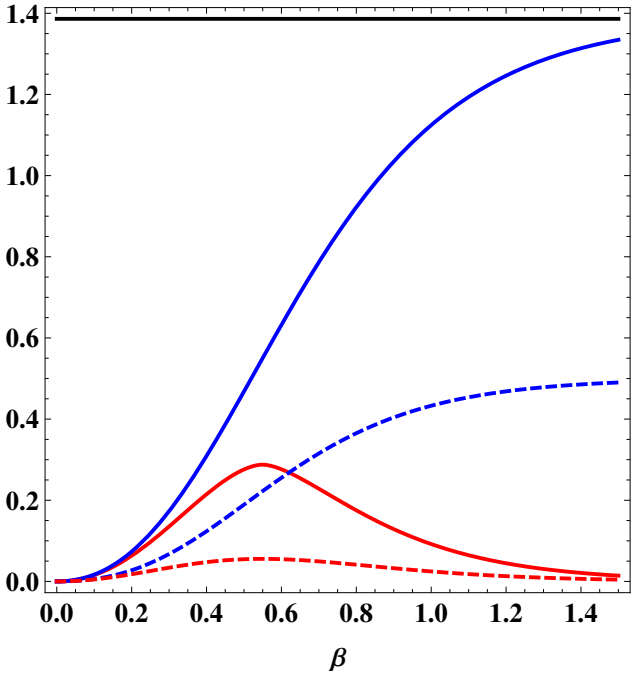

Figure 1. The mutual information and thermo-mutual information in the two-spin system. The solid blue line is the MI and the solid red line is the TMI. The solid black line at the top of the graph denotes $2\log 2$ which is the maximum value of the mutual information. The dashed blue and red lines denote the correlation functions $\frac{1}{2}\left(\langle S^z_{A1}S^z_{B1}\rangle_\Omega\right)^2$ and $\frac{1}{2}\left(\langle S^z_{A1}S^z_{B2}\rangle_\Omega\right)^2$ respectively.

2.5 Computing TMI in field theory

The computation of entanglement entropy in field theories is considerably more involved than in the simple quantum mechanical example above. The standard prescription known as the "replica trick" involves the following steps (see, e.g., [3]). One first constructs a path integral representation of the reduced density matrix $\rho_A := \rho(\Psi; \mathcal{A}(A))$. Using this representation one may compute the "Rényi moments" $\mathrm{tr}_{\mathcal{H}_A}(\rho_A^n)$. This procedure amounts to gluing together path integral representations such that $\mathrm{tr}_{\mathcal{H}_A}(\rho_A^n)$ maybe be viewed as a single path integral over a Riemann surface rather than the original space $\mathcal{M}$. Assuming the expression for $\mathrm{tr}_{\mathcal{H}_A}(\rho_A^n)$ is a complex analytic function of n in a connected region R of the complex n plane which includes the non-negative integers, one may obtain the entanglement entropy $S(\rho_A)$ via

$$S(\rho_A) = -\mathrm{tr}_{\mathcal{H}_A}\rho_A\log\rho_A = -\lim_{n\to 1}\frac{\partial}{\partial n}\mathrm{tr}_{\mathcal{H}_A}(\rho_A^n). \tag{2.36}$$

The path integrals involved in this prescription are on most solid footing in Euclidean signature.

In order to utilize the replica trick to construct both the MI and TMI we need a path integral representation of the reduced density matrices ρ_{A1}, ρ_{B1}, ρ_{B2}, $\rho_{A1\cup B1}$, and $\rho_{A1\cup B2}$. Life is simpler if we work in Euclidean signature $\mathcal{M}\to\mathcal{M}_{\mathrm{E}} = S^1\times\Lambda$ where the Euclidean time circle has radius β. The only subtlety that arises is understanding how type-1 and

JHEP07(2013)081

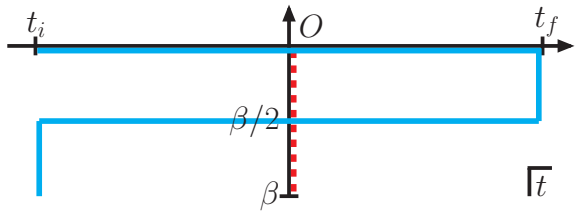

Figure 2. Schwinger-Keldysh time integration contours in the complex t plane. The Euclidean contour is the dashed red line; the TFD contour is the solid blue line. These contours are further discussed in appendix A.

type-2 fields are distinguished in Euclidean signature. Recall that the Euclidean and TFD formulations of thermal field theory are related by a deformation of the Schwinger-Keldysh time contour — see figure 2. From this perspective there are two types of operators in Lorentz signature because the Lorentzian time contour has two legs. However, there is just one leg to the Euclidean time contour and therefore only one set of Euclidean operators. So care must be taken to define the Euclidean analogue of a density matrix in which one type of Lorentzian operators has been traced over. At the end of the day, the Euclidean path integrals defining these density matrices are an intuitive generalization of existing results [3, 4], so we simply quote the results below and relegate a careful derivation to appendix A.

We use as a coordinate on $\mathcal{M}_{\rm E}$ the complex coordinate z with $\mathrm{Re}\, z = x \in \mathbb{R}$ and $\mathrm{Im}\, z \in (-\beta, 0)$. For A a single interval the density matrix ρ_{A1} has the Euclidean path integral representation

$$\rho_{A1}(\psi', \psi) = Z^{-1} \int [\mathcal{D}\phi] e^{-S_{\rm E}[\phi]} \left[\prod_{x \in A} \delta\Big(\phi(0^+) - \psi'(0^+)\Big) \delta\Big(\phi(0^-) - \psi(0^-)\Big) \right]. \quad (2.37)$$

Here ψ', ψ denote Euclidean field profiles and we have labelled only the dependence on $\mathrm{Im}\, z$, i.e., $\phi(0^+) = \phi(\mathrm{Re}\, z, \mathrm{Im}\, z = 0 + i\epsilon)$, etc. Away from the delta function insertions the Euclidean fields $\phi(x)$ satisfy the KMS boundary conditions $\phi(z) \sim \phi(z - i\beta)$. Eq. (2.37) is precisely the path integral obtained from the zero-temperature case by compactifying the Euclidean time direction [4]. The expression for $\rho_{A1 \cup B1}$ follows suit:

$$\rho_{A1\cup B1}(\psi', \psi) = Z^{-1} \int [\mathcal{D}\phi] e^{-S_{\rm E}[\phi]} \left\{ \left[\prod_{x \in A} \delta\Big(\phi(0^+) - \psi'(0^+)\Big) \delta\Big(\phi(0^-) - \psi(0^-)\Big) \right] \right.$$
$$\left. \times \left[\prod_{x \in B} \delta\Big(\phi(0^+) - \psi'(0^+)\Big) \delta\Big(\phi(0^-) - \psi(0^-)\Big) \right] \right\}. \quad (2.38)$$

The path integral for a type-2 density matrix differs from (2.37) in two respects: the delta function insertions are placed at $\mathrm{Im}\, z = -\beta/2$, and the $i\epsilon$ prescriptions are reversed:

$$\rho_{A2}(\psi', \psi) = Z^{-1} \int [\mathcal{D}\phi] e^{-S_{\rm E}[\phi]} \left[\prod_{x \in A} \delta\Big(\phi(-\beta/2 + 0^-) - \psi'(-\beta/2 + 0^-)\Big) \right.$$
$$\left. \times \delta\Big(\phi(-\beta/2 + 0^+) - \psi(-\beta/2 + 0^+)\Big) \right]. \quad (2.39)$$

JHEP07(2013)081

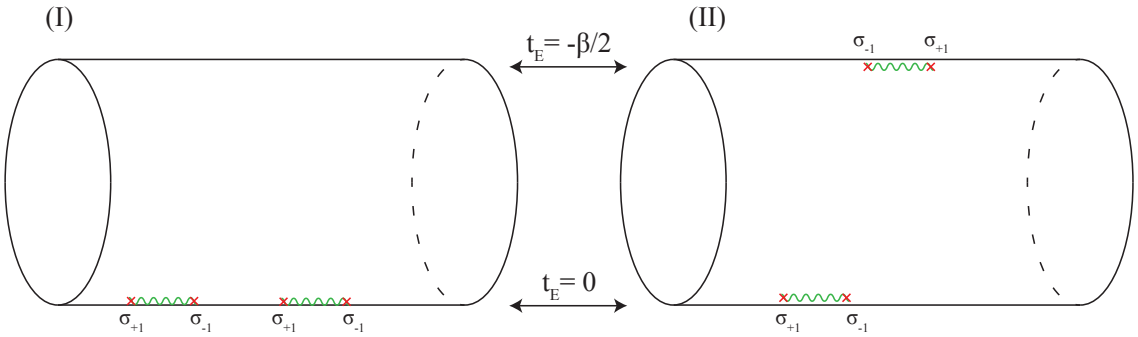

Figure 3. Depiction of the Euclidean path integral (A.12). (I) shows the placement of delta function insertions used to construct the Euclidean analogue of $\rho_{A1\cup B1}$; (II) shows the placement for the Euclidean analogue of $\rho_{A1\cup B2}$. The twist fields (see section 2.6) are also depicted, note that the orientation of the cuts at $-\beta/2$ are reversed.

Of course, using a coordinate transformation one may recast (2.39) in the form of (2.37), so the Rényi moments of ρ_{A1} and ρ_{A2} are equivalent. These differences do matter, however, in the hybrid density matrix:

$$\rho_{A1\cup B2}(\psi',\psi) = Z^{-1}\int[\mathcal{D}\phi]e^{-S_{\rm E}[\phi]}\Bigg\{\Bigg[\prod_{x\in A}\delta\Big(\phi(0^+)-\psi'(0^+)\Big)\delta\Big(\phi(0^-)-\psi(0^-)\Big)\Bigg] \times\Bigg[\prod_{x\in B}\delta\Big(\phi(-i\beta/2+0^-)-\psi'(-i\beta/2+0^-)\Big) \times\delta\Big(\phi(-i\beta/2+0^+)-\psi(-i\beta/2+0^+)\Big)\Bigg]\Bigg\}. \quad (2.40)$$

The placement of delta insertions is depicted in figure 3.

Given (2.37)–(2.40) it is straightforward to proceed with the remaining steps of the replica trick. The result is simply that we study the partition function on a surface constructed by gluing thermal cylinders together, the only difference is that not all cuts are at $\mathrm{Im}\, z = 0$, and the orientation of the cuts at $\mathrm{Im}\, z = -\beta/2$ are reversed. This is a consequence of our $i\epsilon$ prescription, and is reminiscent of calculations of entanglement negativity [27–29], where one exchanges the ordering of twist operators. Both the TMI and negativity are extracted from a correlator $\langle\sigma_+\sigma_-\sigma_-\sigma_+\rangle$, however their locations on the integration contour are quite different: TMI is calculated via

$$\langle\sigma_+(u_1)\sigma_-(v_1)\sigma_-(u_2+i\beta/2)\sigma_+(v_2+i\beta/2)\rangle_\beta \quad (2.41)$$

whereas the "Renyi negativities" are extracted from

$$\langle\sigma_+(u_1)\sigma_-(v_1)\sigma_-(u_2)\sigma_+(v_2)\rangle, \quad (2.42)$$

evaluated on Z_n orbifolds for even n, after which we must analytically continue to $n = 1$.

JHEP07(2013)081

2.6 Example in CFT: 2d massless Dirac fermion

For our second example we consider the $2d$ massless Dirac fermion. This theory is sufficiently simple that, by borrowing heavily from existing results in the literature, we may compute the MI and TMI exactly.

Following the discussion of the previous section, our main task is to compute the Rényi moments $\mathrm{tr}_{\mathcal{H}_C}(\rho_C^n)$ starting from the expression for the Euclidean path integral for ρ_C. We may use the replica trick to glue together path integrals for ρ_C in order to obtain a single path integral for $\mathrm{tr}_{\mathcal{H}_C}(\rho_C^n)$ over an n-sheeted Riemann surface. For 2D CFTs we may use a further refinement of Calabrese and Cardy [4] who have shown that this path integral may be related to the correlation function of twist operators $\sigma_n^{\pm}(z)$ defined on the original space $\mathcal{M}_{\mathrm{E}}$. Let us denote by $[u, v]$ a line on $\mathcal{M}_{\mathrm{E}}$ with endpoints u, v and constant imaginary part, and let C be the union of N disjoint segments $C = \cup_{i=1}^{N}[u_i, v_i]$. The trace $\mathrm{tr}_{\mathcal{H}_C}(\rho_C^n)$ is proportional to a $2N$-pt. correlation function of twist operators:

$$\mathrm{tr}_{\mathcal{H}_C}(\rho_C)^n \propto \langle \sigma_n^{\pm}(u_1)\sigma_n^{\pm}(v_1)\dots\sigma_n^{\pm}(u_N)\sigma_n^{\pm}(v_N)\rangle_{\Omega}. \tag{2.43}$$

The twist operators are conformal primaries with conformal weight

$$\Delta_n = \frac{c}{12}\left(n - \frac{1}{n}\right) = \frac{c}{12}\frac{(n-1)(n+1)}{n}, \tag{2.44}$$

with c the central charge. The choice of which twist field $\sigma_n^{\pm}$ is determined by the placement of the intervals. For the case considered by [4] where all intervals lie on the real axis ($\mathrm{Im}\, z = 0$) the twist correlator is

$$\mathrm{tr}_{\mathcal{H}_C}(\rho_C)^n \propto \langle \sigma_n^{+}(u_1)\sigma_n^{-}(v_1)\dots\sigma_n^{+}(u_N)\sigma_n^{-}(v_N)\rangle_{\Omega}, \quad \mathrm{Im}\, u_i = \mathrm{Im}\, v_i = 0 \;\forall\; i = 1, \dots, N. \tag{2.45}$$

For segments lying on $\mathrm{Im}\, z = -\beta/2$ the orientation of the twist fields is reversed. This is a consequence of the $i\epsilon$ prescriptions described in section 2.5.

In order to compute the MI and TMI we consider the three segments

$$A_1 = [u_{A1}, v_{A1}], \quad \mathrm{Im}\, u_{A1} = \mathrm{Im}\, v_{A1} = 0, \tag{2.46}$$
$$B_1 = [u_{B1}, v_{B1}], \quad \mathrm{Im}\, u_{B1} = \mathrm{Im}\, v_{B1} = 0, \tag{2.47}$$
$$B_2 = [u_{B2}, v_{B2}], \quad \mathrm{Im}\, u_{B2} = \mathrm{Im}\, v_{B2} = -\beta/2, \tag{2.48}$$

The Rényi moments for the associated density matrices are proportional to

$$\mathrm{tr}(\rho_{A1}^n) \propto \langle \sigma_n^{+}(u_{A1})\sigma_n^{-}(v_{A1})\rangle_{\Omega}, \tag{2.49}$$
$$\mathrm{tr}(\rho_{B1}^n) \propto \langle \sigma_n^{+}(u_{B1})\sigma_n^{-}(v_{B1})\rangle_{\Omega}, \tag{2.50}$$
$$\mathrm{tr}(\rho_{B2}^n) \propto \langle \sigma_n^{-}(u_{B2})\sigma_n^{+}(v_{B2})\rangle_{\Omega}. \tag{2.51}$$

These 2-pt. functions are completely determined by conformal symmetry and depend on the specific model only in the value of c which determines Δ_n:

$$\langle \sigma_n^{+}(u_1)\sigma_n^{-}(v_1)\rangle_{\Omega} = \langle \sigma_n^{-}(u_1)\sigma_n^{+}(v_1)\rangle_{\Omega} = \left|\frac{\pi\epsilon}{\beta \sinh\left[\frac{\pi(u_1 - v_1)}{\beta}\right]}\right|^{2\Delta_n}. \tag{2.52}$$

JHEP07(2013)081

The Rényi moments of unions of the regions are proportional to

$$\mathrm{tr}(\rho^n_{A1\cup B1}) \propto \langle \sigma_n^+(u_{A1})\sigma_n^-(v_{A1})\sigma_n^+(u_{B1})\sigma_n^-(v_{B1})\rangle_\Omega, \tag{2.53}$$

$$\mathrm{tr}(\rho^n_{A1\cup B2}) \propto \langle \sigma_n^+(u_{A1})\sigma_n^-(v_{A1})\sigma_n^-(u_{B2})\sigma_n^+(v_{B2})\rangle_\Omega. \tag{2.54}$$

Since the 4-pt. functions are not fully determined by conformal symmetry the right-hand side of these proportionalities are model dependant. For the massless Dirac fermion[3] $c = 1$ and the twist correlators are known [31]:[4]

$$\langle \sigma_n^+(u_1)\sigma_n^-(v_1)\sigma_n^+(u_2)\sigma_n^-(v_2)\rangle_\Omega = \left| \frac{\pi^2\epsilon^2 \sinh\left[\frac{\pi(u_1-u_2)}{\beta}\right]\sinh\left[\frac{\pi(v_1-v_2)}{\beta}\right]}{\beta^2 \sinh\left[\frac{\pi(u_1-v_1)}{\beta}\right]\sinh\left[\frac{\pi(u_1-v_2)}{\beta}\right]\sinh\left[\frac{\pi(v_1-u_2)}{\beta}\right]\sinh\left[\frac{\pi(u_2-v_2)}{\beta}\right]} \right|^{2\Delta_n}, \tag{2.56}$$

$$\langle \sigma_n^+(u_1)\sigma_n^-(v_1)\sigma_n^-(u_2)\sigma_n^+(v_2)\rangle_\Omega = \left| \frac{\pi^2\epsilon^2 \sinh\left[\frac{\pi(u_1-v_2)}{\beta}\right]\sinh\left[\frac{\pi(v_1-u_2)}{\beta}\right]}{\beta^2 \sinh\left[\frac{\pi(u_1-v_1)}{\beta}\right]\sinh\left[\frac{\pi(u_1-u_2)}{\beta}\right]\sinh\left[\frac{\pi(v_1-v_2)}{\beta}\right]\sinh\left[\frac{\pi(u_2-v_2)}{\beta}\right]} \right|^{2\Delta_n}. \tag{2.57}$$

We can now quickly assemble these ingredients into the MI and TMI. The mutual information is given by

$$\mathrm{MI}(A_1 : B_1) = \lim_{n\to 1} \frac{1}{1-n} \log\left[\frac{\mathrm{tr}(\rho^n_{A1})\mathrm{tr}(\rho^n_{B1})}{\mathrm{tr}(\rho^n_{A1\cup B1})}\right] \tag{2.58}$$

We know the Réyni moments up to constants of proportionality which are independent of β. These constants provide an overall constant to the mutual information. The correct value of this constant is fixed by the requirement that the mutual information vanish as $\beta \to 0$. Inserting the expressions for the twist correlators we obtain

$$\mathrm{MI}(A_1 : B_1) = \frac{1}{3}\log\left|\frac{\sinh\left(\frac{\pi(u_{A1}-u_{B1})}{\beta}\right)\sinh\left(\frac{\pi(v_{A1}-v_{B1})}{\beta}\right)}{\sinh\left(\frac{\pi(u_{A1}-v_{B1})}{\beta}\right)\sinh\left(\frac{\pi(v_{A1}-u_{B1})}{\beta}\right)}\right|. \tag{2.59}$$

To clean this expression up consider without loss of generality the configuration $u_{A1} < v_{A1} < u_{B1} < v_{B1}$; we may then adopt the variables

$$|u_{A1} - v_{A1}| = L_A, \quad |u_{B1} - v_{B1}| = L_B, \quad u_{B1} - v_{A1} = S, \tag{2.60}$$

[3] As has been clarified in [30], we will be studying the unprojected Dirac fermion theory, not the modular invariant theory where fermion number is gauged.

[4] For this model the correlation functions of twist fields on the complex plane are given by

$$\langle \sigma_n^+(u_1)\sigma_n^-(v_1)\ldots\sigma_n^+(u_N)\sigma_n^-(v_N)\rangle_{plane} = |\det M|^{2\Delta_n}, \; M_{ij} = \frac{\epsilon}{v_j - u_i}. \tag{2.55}$$

The correlation functions on the cylinder may be obtained by the conformal transformation $w_{plane} = \exp[2\pi z_{cyl}/\beta]$.

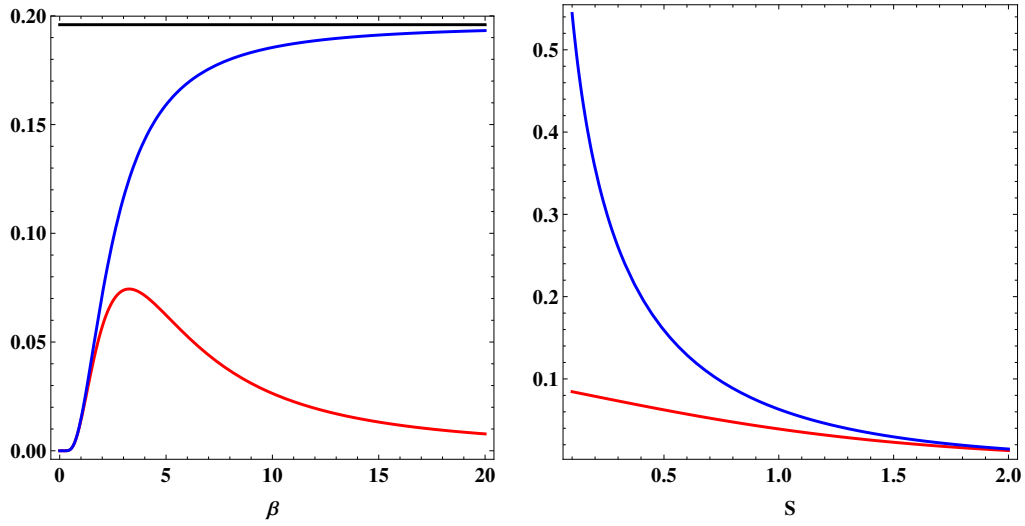

Figure 4. Examples of the MI and TMI of the 2D massless Dirac fermion. Left: the MI (solid blue) and TMI (solid red) as a function of β. In this plot $L_A = L_B = 1$ and $S = 1/2$. The solid black line denotes the maximum value of the MI. Right: the MI and TMI as function of separation S. Here $L_A = L_B = 1$ and $\beta = 5$.

and rewrite (2.59) as

$$\mathrm{MI}(A_1 : B_1) = \frac{1}{3}\log\left[\frac{\sinh\left(\frac{\pi(L_A+S)}{\beta}\right)\sinh\left(\frac{\pi(L_B+S)}{\beta}\right)}{\sinh\left(\frac{\pi(L_A+L_B+S}{\beta}\right)\sinh\left(\frac{\pi S}{\beta}\right)}\right]. \tag{2.61}$$

For the TMI we similarly compute

$$\mathrm{TMI}(A_1 : B_2) = \frac{1}{3}\log\left|\frac{\sinh\left(\frac{\pi(u_{A1}-v_{B2})}{\beta}\right)\sinh\left(\frac{\pi(v_{A1}-u_{B2})}{\beta}\right)}{\sinh\left(\frac{\pi(u_{A1}-u_{B2})}{\beta}\right)\sinh\left(\frac{\pi(v_{A1}-v_{B2})}{\beta}\right)}\right| \tag{2.62}$$

$$= \frac{1}{3}\log\left[\frac{\cosh\left(\frac{\pi(L_A+L_B+S)}{\beta}\right)\cosh\left(\frac{\pi S}{\beta}\right)}{\cosh\left(\frac{\pi(L_A+S)}{\beta}\right)\cosh\left(\frac{\pi(L_B+A)}{\beta}\right)}\right] \tag{2.63}$$

In the second equality we have once again inserted the values (2.60), along with the fact that $\mathrm{Im}\, u_{B2} = \mathrm{Im}\, v_{B2} = -\beta/2$. Once again the overall constant is established by demanding that the TMI vanish as $\beta \to 0$.

We provide representative plots of the MI and TMI in figure 4. As expected, the MI bounds the TMI from above. Both MI and TMI vanish as $\beta \to 0$; as $\beta \to \infty$ the MI approaches is maximum value while the TMI once again vanishes.

3 Holographic thermo-mutual information

In this section we change gears and utilize the holographic techniques of the AdS/CFT correspondence [32] to study TMI from a different perspective. In particular, we use the

JHEP07(2013)081

holographic formula of Ryu and Takayanagi [6] to examine TMI for the $2d$ CFT dual to the non-rotating BTZ black hole in 3 bulk dimensions.

The original RT formula [6] provides a holographic prescription for calculating entanglement entropy in a strongly-coupled d-dimensional CFT on a static spacetime $\mathcal{M}$ which admits a dual description, in the usual sense of AdS/CFT, as a static $d+1$-dimensional asymptotically AdS spacetime $\mathcal{B} = \mathcal{M} \times \mathbb{R}$. Because both bulk and boundary admit a timelike Killing vector ∂_t, we may use the canonical foliation into equal t surfaces $\Sigma_t \subset \mathcal{B}$ and $\partial\Sigma_t \subset \mathcal{M}$. Consider a region $A \subset \partial\Sigma_t$ on the boundary. The RT proposal is that the entanglement entropy S_A is given by[5]

$$S_A = \frac{1}{4G_N} \min_{M_A} \left[\mathrm{Vol}(M_A) \right], \tag{3.1}$$

where $M_A \subset \Sigma_t$ is a surface in the bulk geometry homologous to A. While this is only a conjectured formula, it has passed many nontrivial checks (see e.g. [9, 33, 34] for a review). When the system in question is no longer static (3.1) must be generalized to the covariant holographic entanglement formula of [11]. The clearest presentation of this generalization replaces minimal surfaces with saddlepoints of the area action for spacelike co-dimension two bulk surfaces homologous to A. In 3 bulk geometries these surfaces are simply spacelike geodesics, and the entanglement entropy is then again given by (3.1).

In AdS/CFT thermal systems at high enough temperature and without chemical potential are described by non-rotating eternal black holes. These manifolds have two exterior regions outside the black hole horizon and correspondingly two conformal boundaries, see figure 5. While these manifolds do not admit a global timelike Killing vector field, they do admit Killing vector fields which are timelike in the exterior regions. The AdS/CFT interpretation in this setting was established by Maldacena [17] and in many way follows the classic work of Israel [35]. The two boundaries correspond to the two copies of the CFT in the TFD description of the thermal state. Due to the presence of timelike Killing vector fields on the boundaries the CFT is governed by a time-independent Hamiltonian. The entanglement entropy of the CFT state is realized geometrically as the entropy of the black hole. Basic properties of the TFD system described section 2.2, such as the fact that all type-1 and type-2 operators commute, are clearly realized through this bulk description.

Several authors have used the RT formula to study mutual information in thermal systems holographically (see e.g., [9, 11]). In order to distinguish the holographic prediction from exact results in the field theory we refer to this as the holographic mutual information (HMI). Let ∂_t be the timelike Killing vector field in a exterior region, and consider two regions $A_1, B_1 \subset \partial\Sigma_t$ on the conformal boundary of this exterior region. The HMI between A_1 and B_1 is simply

$$\mathrm{HMI}(A_1 : B_1) := S_{A1} + S_{B1} - S_{A1 \cup B1}, \tag{3.2}$$

with the holographic entanglement entropies computed from the RT formula (3.1). The entropies S_{A1} and S_{B1} are given by $\mathrm{Vol}(M_{A1})$ and $\mathrm{Vol}(M_{B1})$, respectively, where $M_{A1,B1} \subset$

[5] We are working in Einstein frame with the action normalized as $S = \frac{1}{16\pi G_N} \int \sqrt{-g} R + \ldots$ and ignoring higher-derivative corrections.

JHEP07(2013)081

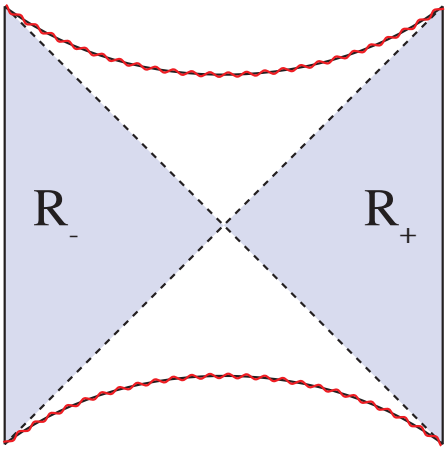

Figure 5. The Penrose-Carter diagram for a maximally extended AdS-Schwarzschild black hole. The two dark shaded regions labeled $R_\pm$ are the regions covered by two AdS-Schwarzschild coordinate patches where the killing vector ∂_t is timelike, bounded by the 45° dashed lines indicating the horizon. The red jagged line is the curvature singularity, which bends inwards for AdS-Schwarzschild black holes in $D > 3$.

Σ_t are the minimal surfaces in the bulk homologous to A_1 and B_1. For the entropy $S_{A1\cup B1}$ there are two candidate minimal surfaces: i) the disconnected surface $M_{A1}\cup M_{B1}$, and ii) the connected minimal surface M_C homologous to $A_1 \cup B_2$. The entropy $S_{A1\cup B1}$ is determined by the lesser volume of these two choices. Thus we may compactly write the HMI as

$$\mathrm{HMI}(A_1 : B_1) = \frac{1}{4G_N} \max\left[\mathrm{Vol}(M_{A1}) + \mathrm{Vol}(M_{B1}) - \mathrm{Vol}(M_C), 0\right], \tag{3.3}$$

where the zero result is obtained when the $S_{A1\cup B1}$ is given by the disconnected minimal surface. It is important to note that none of these surfaces cross the black hole horizon; the geometry behind the horizon is not needed for (or probed by) this computation. This is the analogue of the fact that mutual information may can be constructed from only one copy of the CFT — the second copy is traced out to reproduce the thermal density matrix.

The holographic TMI may be computed in a similar manner to the HMI. Since thermo-mutual information involves operators of both type-1 and type-2, the holographic thermo-mutual information (HTMI) involves regions on each conformal boundary of the extended black hole spacetime. Extended black hole spacetimes do not admit a global timelike Killing vector field, so in general the entanglement entropies must be computed using the covariant form of the RT proposal. As already mentioned, however, in 3 bulk dimensions this does not affect the computation. Let $A_1, B_2 \in \partial\Sigma_t$ be two regions on *different* conformal boundaries. The HTMI between A_1 and B_2 given by

$$\mathrm{HTMI}(A_1 : B_2) = \frac{1}{4G_N} \max\left[\mathrm{Vol}(M_{A1}) + \mathrm{Vol}(M_{B1}) - \mathrm{Vol}(M_C), 0\right], \tag{3.4}$$

where now M_C is the the minimal connected surface connecting A_1 to B_2 which in addition satisfies a regularity condition we describe momentarily. Because there is an Einstein-Rosen

JHEP07(2013)081

bridge connecting the two asymptotic regions, there do indeed exist co-dimension two surfaces which connect A_1 to B_2. In general, finding these minimal surfaces for maximally extended black holes analytically can be difficult; however, in 3 dimensions the computation is much simpler because BTZ black holes are quotients of AdS_3.

The regularity constraint we impose on M_C in the computation of HTMI is the Lorentzian analog of the homology constraint imposed in the RT formula. The homotopy constraint says that, for the geodesics corresponding to $A_1 \cup B_2$, there exists a *spacelike* co-dimension one surface $r_{A1\cup B2}$, in the bulk such that $\partial r = A_1 \cup B_2 \cup M_{A1\cup B2}$. This requirement that the surface is spacelike means that in AdS_3 the ribbon between the geodesics can not twist around, as it would no longer be spacelike. This condition is crucial, as there are configurations where the geodesics corresponding to a twisted ribbon are shorter than the untwisted case (for instance, regions with angular width $\sim \pi$ on opposite sides of the circle) but are rejected due to failing the homology constraint.

We are also not interested in surfaces which wrap the spatial S^1 multiple times - these are guaranteed to be longer than the untwisted "straight across" geodesic, and so can be ignored at leading order.

Before proceding to the compuational details, let us briefly remind the reader of the Hawking-Page [36] phase transition that occurs for AdS black holes at low temperature ($\beta \approx 2\pi$ in conventions defined below). For simplicity we focus on the $2+1$-dimensional case. At high temperatures $\beta \lesssim 2\pi$ the dominant saddle point of the gravity path integral (with asymptotically AdS boundary conditions) is given by the BTZ black hole. In contrast, at low temperature $\beta \gtrsim 2\pi$ the dominant saddlepoint is global AdS. This can be infered, for instance, by comparing the thermodynamic free energy $F = E - TS$ of the two spacetimes:

$$\Delta F = F_{BTZ} - F_{AdS} = -\frac{\pi^2 \ell^2}{2G_N \beta^2} + \frac{1}{8G_N}. \tag{3.5}$$

From this expression one determines that a first-order phase transition occurs at $\beta = 2\pi\ell$. Obviously, the relevant spacetime for use in the RT formula is the dominant saddlepoint. It is clear that in the AdS phase the saddlepoint is two copies of global AdS, with no Einstein-Rosen bridge connecting them, and therefore the TMI will always vanish. Below we focus attention on the high-temperature regime where BTZ provides the correct gravity solution.

3.1 BTZ geometry

This section serves as a brief review of the BTZ geometry. We emphasize the description of BTZ in terms of an embedding space as this formulation makes our computations below quite simple. Similar treatments can be found in [37, 38].

Recall that AdS_3 may be constructed as a 3-dimensional surface in a 4-dimensional embedding space $\mathbb{R}^{2,2}$. Adopting the metric $g_{AB} = \text{diag}\{-,+,+,-\}$, for this space, AdS_3 is the universal cover of the hypersurface defined by

$$-\ell^2 = g_{AB} X^A X^B = -(X^0)^2 + (X^1)^2 + (X^2)^2 - (X^3)^2, \tag{3.6}$$

with ℓ the AdS radius. BTZ is a quotient of AdS_3 and also admits a simple description as an embedded surface. If we identify $X^2 \pm X^3 \cong e^{\pm 4\pi^2/\beta}(X^2 \pm X^3)$ in the embedding space $\mathbb{R}^{2,2}$

JHEP07(2013)081

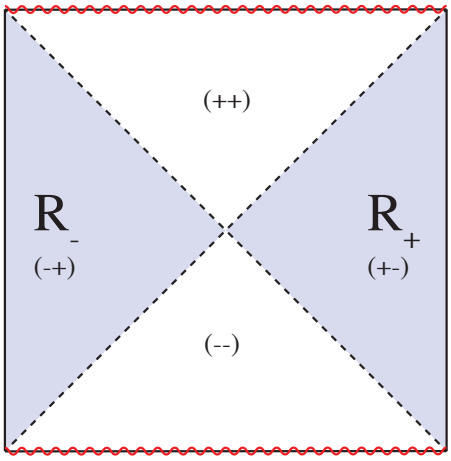

Figure 6. The Penrose-Carter diagram of BTZ. The darker shaded regions are R_+ and R_-, covered by the AdS-Schwarzschild patches (3.10). Note that unlike higher-dimensional black holes, the singularity is not bent in. The $(\cdot,\cdot)$ indicate the signs of w_+ and w_- in each region.

then the BTZ geometry is given by the hypersurface (3.6). We obtain the induced metric on the BTZ geometry by introducing the dimensionless real coordinates (w_+, w_-, ϕ) via

$$\begin{aligned} X^0 &= \ell \left(\frac{-w_+ - w_-}{1 + w_+ w_-} \right), \\ X^1 &= \ell \left(\frac{-w_+ + w_-}{1 + w_+ w_-} \right), \\ X^2 &= \ell \left(\frac{1 - w_+ w_-}{1 + w_+ w_-} \right) \sinh \phi, \\ X^3 &= \ell \left(\frac{1 - w_+ w_-}{1 + w_+ w_-} \right) \cosh \phi. \end{aligned} \tag{3.7}$$

These coordinates have the respective ranges:

$$w_+ \in \mathbb{R}, \quad w_- \in \mathbb{R}, \quad -1 < w_+ w_- < 1, \quad \phi \cong \phi + \frac{4\pi^2}{\beta}. \tag{3.8}$$

The BTZ line element is

$$ds^2 = \frac{\ell^2}{(1 + w_+ w_-)^2} \left[-4 dw_+ dw_- + (-1 + w_+ w_-)^2 d\phi^2 \right]. \tag{3.9}$$

Clearly w_+ and w_- are null coordinates and ϕ is an angular coordinate. There is a conformal boundary at $w_+ w_- = -1$, a horizon at $w_+ w_- = 0$, and a conical singularity at $w_+ w_- = +1$. See figure 6.

For our purposes it is more useful to employ AdS-Schwarzschild coordinates. Consider the regions $R_+ := \{0 \leq w_+, -1 \leq w_+ w_- \leq 0\}$ and $R_- := \{w_+ \leq 0, -1 \leq w_+ w_- \leq 0\}$ respectively; each region is outside the horizon and may be covered by a copy of the AdS-Schwarzschild chart

$$z = z_H \frac{1 + w_+ w_-}{1 - w_+ w_-}, \quad z \in (0, z_H), \quad z_H = \frac{\beta}{2\pi},$$

JHEP07(2013)081

$$
\begin{aligned}
t &= \frac{z_H}{2}\ln\left(-\frac{w_+}{w_-}\right), \quad t \in \mathbb{R}, \\
\theta &= z_H\phi, \quad \theta \cong \theta + 2\pi, \\
w_+ &= \pm\left(\frac{z_H - z}{z_H + z}\right)^{1/2} e^{t/z_H}, \quad w_- = \mp\left(\frac{z_H - z}{z_H + z}\right)^{1/2} e^{-t/z_H}, \qquad (3.10) \\
ds^2 &= \frac{\ell^2}{z^2}\left[-\left(1 - \frac{z^2}{z_H^2}\right)dt^2 + \left(1 - \frac{z^2}{z_H^2}\right)^{-1} dz^2 + d\theta^2\right]. \qquad (3.11)
\end{aligned}
$$

The choice of sign in the last line of (3.10) is $\pm$ for $R_\pm$. We can analytically continue from R_+ to R_- via $t \to t - i\beta/2$. In these coordinates the conformal boundary is at $z = 0$ and the horizon is at $z = z_H$. Using this normalization of time, we see that the horizon has a temperature β^{-1}. The full BTZ geometry also has "upper" and "lower" wedges (recall figure 6); in these regions ∂_t is spacelike.

The extended manifold does not enjoy a global timelike isometry, but it does admit a boost isometry that is timelike in the regions $R_\pm$; the boost vector is

$$
\frac{(1 + w_+w_-)^2}{4w_-}\partial_+ - \frac{(1 + w_+w_-)^2}{4w_+}\partial_- = \frac{\ell^2}{z_H}\partial_t, \qquad (3.12)
$$

which has opposite orientation in the two regions $R_\pm$. Kruskal time $T = \frac{w_+ + w_-}{2}$ provides a global notion of time but ∂_T is not an isometry.

The regions near the conformal boundaries are most easily investigated in the AdS-Schwarzschild charts (3.11). Letting $z = \epsilon$ and taking the limit $\epsilon \to 0$ the other coordinates behave as

$$
\begin{aligned}
w_+ &= \pm(1 - \epsilon/z_H)e^{t/z_H} + \mathcal{O}(\epsilon^2), \\
w_- &= \pm(-1 + \epsilon/z_H)e^{-t/z_H} + \mathcal{O}(\epsilon^2), \\
1 + w_+w_- &= 2\epsilon/z_H + \mathcal{O}(\epsilon^2), \\
1 - w_+w_- &= 2 - 2\epsilon/z_H + \mathcal{O}(\epsilon^2), \qquad (3.13)
\end{aligned}
$$

where the $\pm$ sign is chosen in region $R_\pm$.

3.1.1 Embedding distance

The embedding space endows the BTZ geometry with a convenient notion of distance. We define the *embedding distance* between two points on BTZ to be $\Theta(X, Y) := g_{AB}X^AY^B/\ell^2$. The embedding distance is simply related to the length of the chord through the embedding space

$$
||X - Y||^2 = -2\ell^2(\Theta(X, Y) + 1), \qquad (3.14)
$$

as well as the geodesic distance $D(X, Y)$ on the BTZ manifold:

$$
D(X, Y) = \begin{cases} \ell\,\mathrm{acosh}\,[-\Theta(X, Y)] & \text{spacelike separation} \\ \ell\,\mathrm{acos}\,[-\Theta(X, Y)] & \text{timelike separation.} \end{cases} \qquad (3.15)
$$

JHEP07(2013)081

In the coordinates (3.9) $\Theta(X,Y)$ may be written

$$\Theta(X_1,X_2)=-\frac{2(w_{+1}w_{-2}+w_{-1}w_{+2})+(1-w_{+1}w_{-1})(1-w_{+2}w_{-2})\cosh(\phi_1-\phi_2)}{(1+w_{+1}w_{-1})(1+w_{+2}w_{-2})}. \quad (3.16)$$

Both the embedding distance and geodesic distance generically diverge as one or both points approach the conformal boundaries. Using the limits (3.13) we compute the limit of the embedding distance when both points approach a boundary:

$$\begin{aligned}\Theta(X_1,X_2) &= \frac{\Theta^{\rm reg}(X_1,X_2)}{\epsilon_1\epsilon_2}+\text{finite},\\ \Theta^{\rm reg}(X_1,X_2) &:= z_H^2\left[s(X_1,X_2)\cosh\left(\frac{t_1-t_2}{z_H}\right)-\cosh\left(\frac{\theta_1-\theta_2}{z_H}\right)\right],\end{aligned} \quad (3.17)$$

where $s(X_1,X_2)=+(-)$ for points approaching the same (different) boundaries. For points which are spacelike separated in this limit the geodesic distance behaves as

$$\ell^{-1}D(X_1,X_2)=-\ln(\epsilon_1\epsilon_2)+\ln\left[-2\Theta^{\rm reg}(X_1,X_2)\right]+\ldots, \quad X_1,X_2 \text{ spacelike}, \quad (3.18)$$

with ellipses denoting terms that vanish as $\epsilon_{1,2}\to 0$. In examining these relations it is useful to recall that the AdS-Schwarzschild coordinate t flows in opposite directions on the two boundaries. For instance, under the action of a boost with positive rapidity both t_1 and t_2 increase, regardless of which region the points belong, while the difference t_1-t_2 is unaffected.

3.2 Holographic computation

The embedding space description makes it quite easy to compute both the holographic mutual information and holographic thermo-mutual information. Both quantities may be computed from the dimensionless "cross ratio"

$$J:=\ell^{-1}\left[D(X_{A1},X_{A2})+D(X_{B1},X_{B2})-D(X_{A1},X_{B1})-D(X_{A2},X_{B2})\right], \quad (3.19)$$

which we define for four points X_{A1}, X_{A2}, X_{B1}, X_{B2} in $R_+\cup R_-$. To obtain the HMI let the four points be in R_+ with AdS-Schwarzschild coordinates $X=(t,z,\theta)$:

$$X_{A1}=(0,\epsilon,\theta_{A1}),\quad X_{A2}=(0,\epsilon,\theta_{A2}),\quad X_{B1}=(0,\epsilon,\theta_{B1}),\quad X_{B2}=(0,\epsilon,\theta_{B2}), \quad (3.20)$$

and

$$0\le\theta_{A1}<\theta_{A2}<\theta_{B2}<\theta_{B1}<2\pi. \quad (3.21)$$

The HMI is then given by

$$\text{HMI}(A_1:B_1):=\frac{\ell}{4G_N}\max\left[\lim_{\epsilon\to 0}J,\ 0\right]. \quad (3.22)$$

Taking the limit with the aid of (3.18) and (3.17) we obtain

$$\text{HMI}(A_1:B_1)=\frac{\ell}{4G_N}\ln\max\left[\frac{\left(1-\cosh\frac{\Delta\theta_A}{z_H}\right)\left(1-\cosh\frac{\Delta\theta_B}{z_H}\right)}{\left(1-\cosh\frac{\Delta\theta_1}{z_H}\right)\left(1-\cosh\frac{\Delta\theta_2}{z_H}\right)},\ 1\right], \quad (3.23)$$

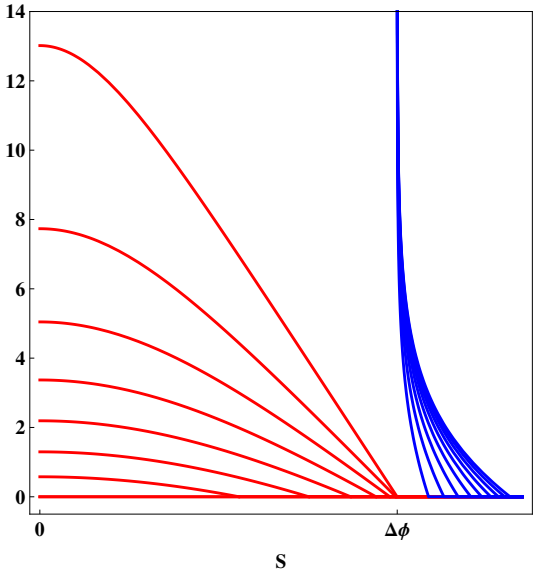

Figure 7. An example of the holographic mutual information (HMI) and thermo-mutual information (HTMI). For this plot the angular widths are $\Delta\phi_A = \Delta\phi_B = \Delta\phi$; S denotes the angular separation between the centers of A and B respectively. In blue are profiles of the HMI for various temperatures, with increasing temperature yielding a non-zero HMI at larger S. In red are profiles of the HTMI for the same temperatures, with increasing temperature yielding greater HTMI. Note that the HTMI vanishes when the θ profiles of A and B have no overlap. For sufficiently low temperature, though still above the Hawking-Page transition, the HTMI vanishes for all S. These features are generic.

where we have introduced the obvious notation

$$\Delta\theta_A = |\theta_{A1} - \theta_{A2}|, \quad \Delta\theta_B = |\theta_{B1} - \theta_{B2}|, \quad \Delta\theta_1 = |\theta_{A1} - \theta_{B1}|, \quad \Delta\theta_2 = |\theta_{A2} - \theta_{B2}|. \tag{3.24}$$

The ordering (3.21) is a convenient choice of labelling so that (3.23) is constructed from the correct choice of geodesics such that the surface M_C is homologous to $A_1 \cup B_1$.

The HTMI is similarly obtained from (3.19) by considering, e.g., $X_{A1}, X_{A2} \in R_+$ and $X_{B1}, X_{B2} \in R_-$. In their respective AdS-Schwarzschild charts the points may once again be labelled by (3.20) with angles satisfying (3.21). This choice of labelling selects the correct surface M_C for defining $S_{A1\cup B2}$ — recall discussion in section 3. The HTMI is then

$$\text{HTMI}(A_1 : B_2) := \frac{\ell}{4G_N} \max\left[\lim_{\epsilon\to 0} J(A:B),\ 0\right], \tag{3.25}$$

and taking the limit we obtain

$$\text{HTMI}(A_1 : B_2) = \frac{\ell}{4G_N} \ln \max\left[\frac{\left(1-\cosh\frac{\Delta\theta_A}{z_H}\right)\left(1-\cosh\frac{\Delta\theta_B}{z_H}\right)}{\left(1+\cosh\frac{\Delta\theta_1}{z_H}\right)\left(1+\cosh\frac{\Delta\theta_2}{z_H}\right)},\ 1\right]. \tag{3.26}$$

As with the thermo-mutual information computed in the quantum mechanics and CFT examples above, the HTMI captures the basic properties of thermo-mutual information outlined in section 2.3, though the agreement is not perfect. In particular we note:

JHEP07(2013)081

i) By construction HTMI is non-negative.

ii) From (3.26) it is clear that HTMI is bounded above for all configurations. The fact that HTMI is constructed from two regions on different boundaries makes it manifest that no UV divergences are encountered when A_1 and B_2 are taken to have overlapping θ profiles.

iii) Given two regions $B_{1,2}$ with equivalent θ profiles, one region on each boundary, we obtain from (3.26) and (3.23) that $\mathrm{HMI}(A_1 : B_1) - \mathrm{HTMI}(A_1 : B_2) \geq 0$. In this sense HTMI bounds HMI from below.

iv) The high temperature limit: when β is much less than all length scales $\Delta\theta_A$, $\Delta\theta_B$, $\Delta\theta_1$, $\Delta\theta_2$, the HTMI becomes

$$\mathrm{HTMI}(A_1 : B_1) \approx \frac{2\pi\ell T}{4G_N} \max\left[(\Delta\theta_A + \Delta\theta_B - \Delta\theta_1 - \Delta\theta_2), 0\right], \tag{3.27}$$

where we have reinstated T for clarity. This expression is non-vanishing when A_1 and B_2 have overlapping θ profile, and in this case $\mathrm{HTMI}(A_1 : B_2) \approx 2s(L/\ell)$, where s is the entropy density and L/ℓ is the length of the overlapping region in AdS units. We conjecture that this behavior is generic and that for any equilibrium finite temperature system, in the high temperature limit $TMI \approx 2s\mathrm{Vol}(\mathrm{overlap})$.

v) Behavior at low temperature: we may readily verify from (3.26) that $\mathrm{HTMI}(A_1 : B_2)$ tends to zero in the limit $\beta \to \infty$. In fact, the HTMI vanishes for $\beta \sim \pi\sqrt{\theta_A\theta_B}$, which can occur well above the Hawking-Page temperature $\beta = 2\pi$. We conjecture that this will occur generically even in higher dimensions.

This last point, the fact that the HTMI can vanish at temperatures well above the Hawking-Page temperature, deserves further discussion. In section 2.3 we made a point to note that at any finite temperature the TMI cannot vanish for all configurations. This follows from the fact that the TMI bounds the correlations of type-1 and type-2 fields, and these correlations cannot everywhere vanish if Ω is indeed entangled. The fact that the HTMI can vanish for typical regions at finite temperature is a large N artifact. Recall that the RT formula is believed to capture only the $\mathcal{O}(N^2)$ contributions to the entanglement entropies. Therefore the HTMI is itself contains only the leading large N behavior of the TMI. Correlations between type-1 and type-2 fields are naturally $\mathcal{O}(N^0)$ are therefore are technically zero at this order. We provide a representative plot of HTMI and HMI in figure 7.

4 Discussion

In this paper we have studied thermo-mutual information (TMI), an analogue of mutual information which provides a measure for the correlation between 'physical' and thermo-double degrees of freedom. The basic attributes of TMI may be determined directly from its definition in thermal QFT, are quite analogous to those of mutual information, and are summarized in section 2.3. We highlight in particular that TMI is a UV-finite quantity in

JHEP07(2013)081

field theory is "universal" (i.e. UV regulator-independent) and is well-defined for any theory local enough to factor the Hilbert space or operators. Through the Pinsker inequality (2.25) TMI provides an upper bound on the correlation functions between type-1 and type-2 operators inserted at arbitrary separations. As a result, TMI carries much more qualitative information about a state of a theory than the entropy of the mixed state and has different information than the mutual information. We have explored TMI in detail in three examples: a two-site spin chain, a 2d Dirac fermion, and a 2d CFT described by a holographic dual.

It is natural to ask what the possible applications of TMI are within thermal field theory. As a simple calculation, consider the computation of correlators in the thermal vacuum using canonical perturbation theory about small couplings. In this setting the correlation function $\langle\phi_1(x)\phi_2(y)\rangle_\Omega$ provides one of the Schwinger-Keldysh Green's functions. TMI may be used to estimate the strength of perturbative corrections; in particular, TMI may be used to bound from above the smooth, UV-finite part of Feynman diagrams arising from the coupling between type-1 and type-2 fields. Similarly, TMI may be used to bound the smooth part of retarded and advanced thermal Green's functions.

Of course, our primary motivation for introducing TMI was so that we could study it holographically via AdS/CFT. There are several reasons for this. First, we note that holographic TMI provides yet another test of the conjectured Ryu-Takayanagi formula [6]. Indeed, as described in section 2.3, holographic TMI has all the hallmarks of a TMI in (large N) field theory. Certainly more interesting is the fact that holographically-computed TMI provides the simplest example of holographic mutual information between regions on disconnected AdS boundaries. In general, the dual CFT description of AdS spaces with multiple boundaries is poorly understood. It is reasonable to expect that holographic mutual information can provide basic information about the CFT which describes these bulk spacetimes. Perhaps the most obvious example is to note that holographic mutual information, if it indeed provides a measure of mutual information in the dual CFT, bounds the correlations between operators on different boundaries.

In general the agreement between the holographically-computed TMI and our expectations from QFT is quite good, but we should comment on the most significant discrepancy: the holographic TMI can vanish for any choice of region at finite temperature, contrary the definition of TMI. This is due to the fact that the holographic computation captures only the leading behavior in N^2, and so like the holographic mutual information exhibits features similar to a first order phase transition. Indeed, that it is precisely the same phenomena as for the holographic mutual information may be seen as follows. One may adopt Rindler coordinates on the boundary of global AdS and in doing so describe the zero-temperature pure state (from the global perspective) as a thermal state at the Rindler temperature. The CFT in one Rindler wedge may be interpreted in the TFD language as the thermo-double of the the CFT in the other wedge. In this set-up the thermo-mutual information is precisely the mutual information of the global perspective.

We close with a discussion of some possible future directions of research.

JHEP07(2013)081

4.1 Holographic TMI in higher dimensions

A natural extension of this work would be to examine holographic TMI computed in higher dimensional black hole backgrounds. While conceptually a straight-forward generalization, the necessary computations are considerably more involved in $d+1$ bulk dimensions with $d > 2$. Partly this is due to the fact that in higher dimensions the covariant form of the RT formula is necessary and the extremal surfaces involved have dimension greater than two. In addition, in $2+1$ bulk dimensions our computations were rather slick because of the fact that BTZ is a quotient of AdS_3. Regardless of these computational challenges, we expect similar physics in higher dimensions. Namely, we expect the holographically computed TMI to be non-vanishing even at leading order in N^2, and we expect it to exhibit a first order phase transition at $\beta \sim \pi L$ where L is the length scale of the regions under consideration. The features of TMI listed in section 2.3 are of course independent of dimension.

4.2 Other asymptotically-AdS geometries

It has been pointed out by several authors [39–43] that in $2+1$ Einstein gravity the maximally extended BTZ geometry is not the only solution which has one asymptotic region corresponding to that of the AdS-Schwarzschild chart (3.11). There also exist solutions with more than two asymptotic regions as well as those with only one asymptotic region but non-trivial topology behind the horizon. We expect holographically-computed mutual information between regions on separate boundaries to be useful in characterizing the CFT dual description of these spacetimes. Geometries with more than two asymptotic regions may be thought of as describing different choices of purification for a system initially described by a thermal density matrix. These purifications enlarge the total Hilbert space to a space other than the TFD Hilbert space $\mathcal{H}^{\otimes 2}$. Basic features of these purifications may be determined by examining HTMI-like mutual information "correlators."

Solutions with only one asymptotic region but non-trivial topology are even more fascinating. The AdS/CFT intuition states that the CFT dual of these geometries must be in a pure state. However, the RT formula applied in any black hole spacetime predicts a mixed state: due to the presence of the black hole in the bulk, the RT formula computes for any region A that $S_A \neq S_{\bar{A}}$, indicating that the state is mixed. For these spacetimes it appears that the RT formula gives the incorrect result at leading order in N^2, but this warrants a more careful analysis.

4.3 Renormalized entanglement entropy and mutual information

We have emphasized throughout our analysis that one important reason mutual information (and, for intersecting regions, the F-function) is an object of interest is that it is a manifestly UV finite quantity. Recently [44] has proposed a UV-finite "renormalized entanglement entropy" (REE). It is interesting to ask if the same physics contained the MI may also be recovered from linear combinations of the REE. For a 2d system [44] define the REE for a subregion A with length scale L to be $\mathcal{S}_A = L\partial_L S_A$. The naive "renormalized mutual information" is then $L\partial_L(S_A + S_B - S_{A\cup B})$. However, this quantity does not appear to capture the same physics; in particular, the derivative with respect to L annihilates

JHEP07(2013)081

the dependence on the scale-invariant cross-ratio. For zero temperature CFTs the mutual information is a function only of this cross-ratio, so this renormalized mutual information vanishes. For CFTs at finite temperature the naive renormalized mutual information is non-zero but again does not depend on the cross-ratio and so does not contain information about correlations, only information about the geometries under consideration. We mention this here in the hope that it spurs a better understanding of the relationship between the proposed REE and the UV-finite quantities considered in our analysis.

Acknowledgments

We thank Matthew Headrick, Matthew Kleban, Alex Maloney, Guy Moore, and Massimo Porrati for useful discussions. MMR would like to thank Hurricane Sandy for a stimulating work environment while this project was being completed. IAM and MMR are supported by the Simons Postdoctoral Fellowship Program.

A Euclidean path integrals for reduced density matrices in TFD

In this appendix we derive the results quoted in section 2.5. We begin by reviewing the relationship between the TFD path integral and the Euclidean path integral. Boundary conditions must be supplied in order for any path integral expression to be well-defined; for thermal systems the relevant boundary condition is the KMS condition [45]. Denoting the time translation of ϕ by $\phi(t) = e^{iHt}\phi(0)e^{-iHt}$ and suppressing other spacetime arguments, one readily deduces from (2.10) that correlators of the thermal state Ω at inverse temperature β satisfy

$$\langle \phi(t)\chi\rangle_\Omega = \langle \chi\phi(t+i\beta)\rangle_\Omega, \tag{A.1}$$

for two operators $\phi(x)$ and $\chi(x)$. A consequence of (A.1) is that correlators with respect to Ω are boundary values of analytic functions in the complex time domain $\mathrm{Im}\, t \in (0, -\beta)$ satisfying the condition (A.1). Therefore we may seek a path integral generating function $Z_C[J]$ for the path-ordered correlation functions $\langle P\phi(x_1)\dots\phi(x_n)\rangle_\Omega$. The 'path' refers to the time integration which is traversed from $\mathrm{Im}\, t = 0$ to $\mathrm{Im}\, t = -\beta$ along a contour C; a more careful examination of the analyticity properties of such correlators reveals that the path must have monotonically non-increasing $\mathrm{Im}\, t$ [24]. The path integral may be constructed in the usual manner:

$$Z_C[J] := Z^{-1}\int [\mathcal{D}\phi]\, \exp\left[iS_C[\phi] + i\int_C dt \int d^{D-1}x\sqrt{-g(x)}J(x)\phi(x)\right], \tag{A.2}$$

D is the number of spacetime dimensions and $Z = Z[0]$. The subscript $S_C[\phi]$ denotes that, like the source term written explicitly in (A.2), the time integration in the action is over the path C. The boundary conditions imposed on the field integration is $\phi(t) = \phi(t+i\beta)$. Path-ordered correlation functions may be computed by taking functional derivatives with respect to the source $J(x)$:

$$\langle P\phi(x_1)\dots\phi(x_n)\rangle_\Omega = \left.\frac{\delta^n Z_C[J]}{i\delta J(x_1)\cdots i\delta J(x_n)}\right|_{J=0}. \tag{A.3}$$

JHEP07(2013)081

The two choices of time contour relevant for our discussion are shown in figure 2. The first choice is the Euclidean contour which is traversed along the imaginary t axis $0 \to -i\beta$. This path integral determines the Euclidean correlators $\langle \phi(x_1) \dots \phi(x_n) \rangle_{\rm E}$ which define the Euclidean 'state.' Explicitly,

$$Z_{\rm E}[J] := Z^{-1} \int [\mathcal{D}\phi] \, \exp\left[-S_{\rm E}[\phi] - \int_{-\beta}^{0} d\tau \int d^{D-1}x \sqrt{g(x)} J(x)\phi(x) \right]. \tag{A.4}$$

A second time contour is the TFD contour — see figure 2. With t_i and t_f real initial and final times respectively, this contour is traversed: i) $t_i \to t_f$, ii) $t_f \to t_f - i\beta/2$, iii) $t_f - i\beta/2 \to t_i - i\beta/2$, iv) $t_i - i\beta/2 \to t_i - i\beta$. Under reasonable circumstances (see discussion section 2.4 of [24]) the path integral factorizes into two path integrals, one involving the horizontal legs of the contour, the other involving the vertical legs. If one is interested only in correlators of operators lying on the horizontal contours then the latter path integral is simply 1 due to the overall normalization. The path integral for the horizontal segments is

$$\begin{aligned} Z_{\rm TFD}[J_1, J_2] := Z_{\rm TFD}^{-1} \int [\mathcal{D}\phi_1][\mathcal{D}\phi_2] \, \exp\Bigg[& + iS[\phi_1] - iS[\phi_2] \\ & + i \int d^D x \sqrt{g(x)} \left(J_1(x)\phi_1(x) - J_2(x)\phi_2(x) \right) \Bigg]. \end{aligned} \tag{A.5}$$

Here $\phi_1(x)$ denote fields on the real axis while $\phi_2(x)$ fields have $\mathrm{Im}\, t = -\beta/2$. As our notation implies, these fields correspond to the type-1 and type-2 operators described in section 2.2. Correlators of the operators are generated via:

$$\begin{aligned} & \langle [T\phi_1(x_1) \dots \phi_1(x_n)] \, [\overline{T}\phi_2(y_1) \dots \phi_2(y_m)] \rangle_\Omega \\ & \qquad = \frac{\delta^{n+m} Z_{\rm TFD}[J_1, J_2]}{i\delta J_(x_1) \cdots i\delta J_1(x_n)(-i)\delta J_2(y_1) \cdots (-i)\delta J_2(y_m)} \Bigg|_{J_1 = J_2 = 0}. \end{aligned} \tag{A.6}$$

We may now construct path integral representations of a reduced density matrix in the TFD system. Let us first consider the density operator $\rho_{A1} = \rho(\Omega; \mathcal{A}_1(A))$. Without loss of generality we let the region $A \subset \Sigma_0$. For a basis in $\mathcal{H}_{A1}$ we use the set of states $\{\psi_{A1}\}$ specified by their field configuration of type-1 fields $\psi_1(x)$ on A:

$$\psi_{A1} := \{ \phi_1(x) = \psi_1(x) \mid x \in A \}. \tag{A.7}$$

We denote the matrix elements of ρ_{A1} in this basis $\rho_{A1}(\psi'_{A1}|\psi_{A1})$. Following [3], the path integral representation of $\rho_{A1}(\psi'_{A1}|\psi_{A1})$ is then easily constructed by inserting delta functionals into the path integral (A.5):

$$\begin{aligned} \rho_{A1}(\psi'_{A1}|\psi_{A1}) = Z^{-1} \int [\mathcal{D}\phi_1][\mathcal{D}\phi_2] \Bigg\{ & \exp\left[+iS[\phi_1] - iS[\phi_2] \right] \\ & \times \left[\prod_{x \in A} \delta(\phi_1(0^+) - \psi'_1(0^+)) \delta(\phi_1(0^-) - \psi_1(0^-)) \right] \Bigg\}. \end{aligned} \tag{A.8}$$

JHEP07(2013)081

We have suppressed the dependence of spatial coordinates. The limits $0^{\pm}$ denote how t should be taken to approach $t = 0$, and reflect the fact that we define ψ' (ψ) in the limit $t \to 0^{+(-)}$. The analogous expression for the density matrix ρ_{A2}, in an analogous basis $\{\psi_{A2}\}$, is

$$\begin{aligned}\rho_{A2}(\psi'_{A2}|\psi_{A2}) = Z^{-1}\int[\mathcal{D}\phi_1][\mathcal{D}\phi_2]\Bigg\{ &\exp\left[+iS[\phi_1] - iS[\phi_2]\right] \\ &\times\Bigg[\prod_{x\in A}\delta(\phi_2(-i\beta/2+0^+) - \psi'_2(-i\beta/2+0^+)) \\ &\times\delta(\phi_2(-i\beta/2+0^-) - \psi_2(-i\beta/2+0^-))\Bigg]\Bigg\}. \end{aligned} \tag{A.9}$$

The density matrices $\rho_{A1\cup B1}$ and $\rho_{A1\cup B2}$ are constructed from the obvious generalizations of these expressions.

We would like to compute these path integrals in Euclidean signature; this requires that we deform the TFD time contour to the Euclidean contour. To do so we recast the $t + 0^{\pm}$ limits in the expressions above in terms of path ordering rather than real time ordering. Let $\lambda(t)$ denote a function that decreases monotonically along the path from t_i to $t_i - i\beta$. By rewriting the TFD path integral in terms of $\lambda(t)$ it is then straightforward to deform the time contour to the Euclidean contour. We then let $\lambda = \mathrm{Im}\, t$. For instance, after performing this step we obtain a Euclidean expression for the density matrix ρ_{A1}:

$$\rho^{\mathrm{E}}_{A1}(\psi'_A|\psi_A) = Z^{-1}\int[\mathcal{D}\phi]\, e^{-S_{\mathrm{E}}[\phi]}\Bigg[\prod_{x\in A}\delta(\phi(0^-) - \psi'_1(0^-))\delta(\phi(0^+) - \psi_1(0^+))\Bigg], \tag{A.10}$$

where now we label only the dependence on $\mathrm{Im}\, t$. By the same steps we obtain the analogue of ρ_{A2}:

$$\begin{aligned}\rho^{\mathrm{E}}_{A2}(\psi'_A|\psi_A) = Z^{-1}\int[\mathcal{D}\phi]\, e^{-S_{\mathrm{E}}[\phi]}\Bigg[&\prod_{x\in A}\delta(\phi(-\beta/2+0^+) - \psi'_2(-\beta/2+0^+)) \\ &\times\delta(\phi(-\beta/2+0^-) - \psi_2(-\beta/2+0^-))\Bigg]. \end{aligned} \tag{A.11}$$

Notice that the $i\epsilon$ prescriptions defining the states have switched. Finally, we record the formula for the Euclidean analogue of the density matrix $\rho_{A1\cup B2}$. This is the key formula necessary to compute the thermo-mutual information via the replica trick:

$$\begin{aligned}&\rho^{\mathrm{E}}_{A1\cup B2}(\psi'|\psi) \\ &= Z^{-1}\int[\mathcal{D}\phi]\, e^{-S_{\mathrm{E}}[\phi]}\Bigg\{\Bigg[\prod_{x\in A}\delta(\phi(0^-) - \psi'(0^-))\delta(\phi(0^+) - \psi(0^+))\Bigg] \\ &\qquad\times\Bigg[\prod_{x\in B}\delta(\phi(-\beta/2+0^+) - \psi'(-\beta/2+0^+)) \\ &\qquad\qquad\times\delta(\phi(-\beta/2+0^-) - \psi(-\beta/2+0^-))\Bigg]\Bigg\}. \end{aligned} \tag{A.12}$$

References

[1] B. Groisman, S. Popescu and A. Winter, *Quantum, classical and total amount of correlations in a quantum state*, *Phys. Rev.* **A 72** (2005) 032317 [quant-ph/0410091].

[2] M.M. Wolf, F. Verstraete, M.B. Hastings and J.I. Cirac, *Area laws in quantum systems: mutual information and correlations*, *Phys. Rev. Lett.* **100** (2008) 070502 [arXiv:0704.3906].

[3] P. Calabrese and J.L. Cardy, *Entanglement entropy and quantum field theory*, *J. Stat. Mech.* **06** (2004) P06002 [hep-th/0405152] [INSPIRE].

[4] P. Calabrese and J. Cardy, *Entanglement entropy and conformal field theory*, *J. Phys.* **A 42** (2009) 504005 [arXiv:0905.4013] [INSPIRE].

[5] H. Casini and M. Huerta, *Entanglement entropy in free quantum field theory*, *J. Phys.* **A 42** (2009) 504007 [arXiv:0905.2562] [INSPIRE].

[6] S. Ryu and T. Takayanagi, *Holographic derivation of entanglement entropy from AdS/CFT*, *Phys. Rev. Lett.* **96** (2006) 181602 [hep-th/0603001] [INSPIRE].

[7] G. Michalogiorgakis, *Entanglement entropy of two dimensional systems and holography*, *JHEP* **12** (2008) 068 [arXiv:0806.2661] [INSPIRE].

[8] A. Schwimmer and S. Theisen, *Entanglement entropy, trace anomalies and holography*, *Nucl. Phys.* **B 801** (2008) 1 [arXiv:0802.1017] [INSPIRE].

[9] M. Headrick, *Entanglement Renyi entropies in holographic theories*, *Phys. Rev.* **D 82** (2010) 126010 [arXiv:1006.0047] [INSPIRE].

[10] H. Casini, M. Huerta and R.C. Myers, *Towards a derivation of holographic entanglement entropy*, *JHEP* **05** (2011) 036 [arXiv:1102.0440] [INSPIRE].

[11] V.E. Hubeny, M. Rangamani and T. Takayanagi, *A covariant holographic entanglement entropy proposal*, *JHEP* **07** (2007) 062 [arXiv:0705.0016] [INSPIRE].

[12] V.E. Hubeny, *Extremal surfaces as bulk probes in AdS/CFT*, *JHEP* **07** (2012) 093 [arXiv:1203.1044] [INSPIRE].

[13] V.E. Hubeny and M. Rangamani, *Causal holographic information*, *JHEP* **06** (2012) 114 [arXiv:1204.1698] [INSPIRE].

[14] B. Czech, J.L. Karczmarek, F. Nogueira and M. Van Raamsdonk, *The gravity dual of a density matrix*, *Class. Quant. Grav.* **29** (2012) 155009 [arXiv:1204.1330] [INSPIRE].

[15] R. Bousso, S. Leichenauer and V. Rosenhaus, *Light-sheets and AdS/CFT*, *Phys. Rev.* **D 86** (2012) 046009 [arXiv:1203.6619] [INSPIRE].

[16] D. Marolf and A.C. Wall, *Eternal black holes and superselection in AdS/CFT*, *Class. Quant. Grav.* **30** (2013) 025001 [arXiv:1210.3590] [INSPIRE].

[17] J.M. Maldacena, *Eternal black holes in anti-de Sitter*, *JHEP* **04** (2003) 021 [hep-th/0106112] [INSPIRE].

[18] H. Casini, *Geometric entropy, area and strong subadditivity*, *Class. Quant. Grav.* **21** (2004) 2351 [hep-th/0312238] [INSPIRE].

[19] H. Casini and M. Huerta, *A finite entanglement entropy and the c-theorem*, *Phys. Lett.* **B 600** (2004) 142 [hep-th/0405111] [INSPIRE].

[20] J. Eisert, M. Cramer and M. Plenio, *Area laws for the entanglement entropy — a review*, *Rev. Mod. Phys.* **82** (2010) 277 [arXiv:0808.3773] [INSPIRE].

JHEP07(2013)081

[21] G. Refael and J.E. Moore, *Criticality and entanglement in random quantum systems*, *J. Phys.* **A 42** (2009) 4010 [arXiv:0908.1986].

[22] J.S. Schwinger, *Brownian motion of a quantum oscillator*, *J. Math. Phys.* **2** (1961) 407 [INSPIRE].

[23] L. Keldysh, *Diagram technique for nonequilibrium processes*, *Zh. Eksp. Teor. Fiz.* **47** (1964) 1515 [*Sov. Phys. JETP* **20** (1965) 1018] [INSPIRE].

[24] N. Landsman and C. van Weert, *Real and imaginary time field theory at finite temperature and density*, *Phys. Rept.* **145** (1987) 141 [INSPIRE].

[25] Y. Takahashi and H. Umezawa, *Thermo field dynamics*, *Int. J. Mod. Phys.* **B 10** (1996) 1755 [INSPIRE].

[26] J.J. Sakurai, *Modern quantum mechanics (revised edition)*, first edition, Addison Wesley, U.S.A. (1993).

[27] P. Calabrese, J. Cardy and E. Tonni, *Entanglement negativity in extended systems: a field theoretical approach*, *J. Stat. Mech.* **02** (2013) P02008 [arXiv:1210.5359] [INSPIRE].

[28] P. Calabrese, J. Cardy and E. Tonni, *Entanglement negativity in quantum field theory*, *Phys. Rev. Lett.* **109** (2012) 130502 [arXiv:1206.3092] [INSPIRE].

[29] A.K. Das, *Finite temperature field theory*, World Scientific Publishing Company, Singapore (1997).

[30] M. Headrick, A. Lawrence and M. Roberts, *Bose-Fermi duality and entanglement entropies*, *J. Stat. Mech.* **02** (2013) P02022 [arXiv:1209.2428] [INSPIRE].

[31] H. Casini, C. Fosco and M. Huerta, *Entanglement and alpha entropies for a massive Dirac field in two dimensions*, *J. Stat. Mech.* **07** (2005) P07007 [cond-mat/0505563] [INSPIRE].

[32] O. Aharony, S.S. Gubser, J.M. Maldacena, H. Ooguri and Y. Oz, *Large-N field theories, string theory and gravity*, *Phys. Rept.* **323** (2000) 183 [hep-th/9905111] [INSPIRE].

[33] T. Nishioka, S. Ryu and T. Takayanagi, *Holographic entanglement entropy: an overview*, *J. Phys.* **A 42** (2009) 504008 [arXiv:0905.0932] [INSPIRE].

[34] P. Hayden, M. Headrick and A. Maloney, *Holographic mutual information is monogamous*, *Phys. Rev.* **D 87** (2013) 046003 [arXiv:1107.2940] [INSPIRE].

[35] W. Israel, *Thermo field dynamics of black holes*, *Phys. Lett.* **A 57** (1976) 107 [INSPIRE].

[36] S. Hawking and D.N. Page, *Thermodynamics of black holes in anti-de Sitter space*, *Commun. Math. Phys.* **87** (1983) 577 [INSPIRE].

[37] P. Kraus, H. Ooguri and S. Shenker, *Inside the horizon with AdS/CFT*, *Phys. Rev.* **D 67** (2003) 124022 [hep-th/0212277] [INSPIRE].

[38] L. Fidkowski, V. Hubeny, M. Kleban and S. Shenker, *The black hole singularity in AdS/CFT*, *JHEP* **02** (2004) 014 [hep-th/0306170] [INSPIRE].

[39] S. Aminneborg, I. Bengtsson, D. Brill, S. Holst and P. Peldan, *Black holes and wormholes in* $(2+1)$*-dimensions*, *Class. Quant. Grav.* **15** (1998) 627 [gr-qc/9707036] [INSPIRE].

[40] D. Brill, *Black holes and wormholes in* $(2+1)$*-dimensions*, gr-qc/9904083 [INSPIRE].

[41] K. Krasnov, *Holography and Riemann surfaces*, *Adv. Theor. Math. Phys.* **4** (2000) 929 [hep-th/0005106] [INSPIRE].

JHEP07(2013)081

[42] K. Krasnov, *Black hole thermodynamics and Riemann surfaces*, *Class. Quant. Grav.* **20** (2003) 2235 [gr-qc/0302073] [INSPIRE].

[43] K. Skenderis and B.C. van Rees, *Holography and wormholes in* $2+1$ *dimensions*, *Commun. Math. Phys.* **301** (2011) 583 [arXiv:0912.2090] [INSPIRE].

[44] H. Liu and M. Mezei, *A refinement of entanglement entropy and the number of degrees of freedom*, arXiv:1202.2070 [INSPIRE].

[45] R. Haag, N. Hugenholtz and M. Winnink, *On the equilibrium states in quantum statistical mechanics*, *Commun. Math. Phys.* **5** (1967) 215 [INSPIRE].

JHEP07(2013)081